Scientific
Research

Gravity Survey on the Mizuho Plateau, East Antarctica: SEAL Seismic Exploration in 2001-2002

Shigeru Toda[1*], Hiroki Miyamachi[2], Masaki Kanao[3], Takeshi Matsushima[4], Masamitsu Takada[5], Atsushi Watanabe[6], Mikiya Yamashita[7]

[1]Department of Earth Sciences, Faculty of Education, Aichi University of Education, Kariya, Japan
[2]Department of Earth and Environmental Sciences, Faculty of Science, Kagoshima University, Kagoshima, Japan
[3]National Institute of Polar Research, Tokyo, Japan
[4]Shimabara Observatory, Institute of Seismology and Volcanology, Faculty of Sciences, Kyushu University, Shimabara, Japan
[5]Institute of Seismology and Volcanology, Graduate School of Science, Hokkaido University, Sapporo, Japan
[6]Earthquake Research Institute, The University of Tokyo, Tokyo, Japan
[7]Institute for Research on Earth Evolution, Japan Agency for Marine-Earth Science and Technology, Yokohama, Japan
Email: [*]shigeru@auecc.aichi-edu.ac.jp, miya@sci.kagoshima-u.ac.jp, kanao@nipr.ac.jp, mat@sevo.kyushu-u.ac.jp, takada@sci.hokudai.ac.jp, atsushi@eri.u-tokyo.ac.jp, mikiya@jamstec.go.jp

ABSTRACT

A gravity survey on Mizuho Plateau was carried out in austral summer of 2001-2002 by the 43rd Japanese Antarctic Research Expedition (JARE-43), as one of the geophysical measurements of deep seismic exploration. Gravity measurements were conducted at 151 points in approximately 1 km interval along the 150 km profile. Considering the gravity effect from the ice-sheet, Free-air and Bouguer anomalies were calculated by using precise GPS locations. Furrowed and basin-like negative Free-air anomalies were observed in middle and northern parts of the profile. Bouguer anomalies were calculated by two bedrock elevation data obtained from seismic refraction and radio-echo sounding. High resolution model for bedrock elevation by radio-echo sounding was applied in determining the crustal thickness.

KEYWORDS

1. Introduction

Several geophysical investigations have been carried out to understand the physical characteristics beneath the continental ice-sheet on Mizuho Plateau, East Antarctica by the Japanese Antarctic Research Expedition (JARE). The Mizuho Plateau is a part of the Paleozoic Lützow-Holm Complex (LHC), which is known as a region which experienced a metamorphic event in 550 Ma [1]. Before this study, land traverse gravity surveys were conducted for several times on the Plateau since 1961 [2-5]. A significant inclination of the Moho discontinuity from inland plateau area to the coast along the Mizuho—

Dome-F routes was analyzed by the previously obtained gravity data [6]. In these previous studies, however, a station spacing of the gravity measurements was about a few km or larger, therefore it requires that the station interval be more dense to address detail discussion about the fine structure.

A multidisciplinary geosciences project on "Structure and Evolution of the East Antarctic Lithosphere (SEAL)" had been conducted in the Western Enderby Land—Eastern Dronning Maud Land in a framework of JARE [7,8]. As a main component of the SEAL project, the JARE-41 conducted deep seismic exploration (refraction and wide-angle reflection surveys), as well as the gravity measurements with a dense station distribution along the

---
[*]Corresponding author.

Mizuho traverse routes in austral summer of 1999-2000 [9]. A P-wave velocity structure of the ice-sheet and uppermost crustal layer along the profile were obtained by analyzing the recorded travel-time data [10]. [11] obtained gravity anomalies beneath the Mizuho traverse routes. The estimated density model by [11] indicates that the Moho discontinuity slightly declines about 1 km from coast to inland over 200 km in length.

In succession to the JARE-41 field operation, a similar seismic exploration was held on the Mizuho Plateau by the JARE-43 in austral summer of 2001-2002. The specifications of the seismic observations and instrumentations were the same as those of JARE-41. The survey profile of JARE-43 intersects the JARE-41 profile at "H176" point and spreads out to NNE-SSW direction with 150 km in length (**Figure 1**). More detailed specifications of the JARE-43 seismic surveys are referred to [12]. Dense gravity measurements were also conducted along the JARE-43 profile. In this paper, we represent the details of the gravity measurements, and demonstrate the obtained Free-air and Bouguer gravity anomalies along the survey line by JARE-43.

2. Gravity Survey

2.1. Gravity Measurements

The land traverse gravity measurements were conducted using a SCINTREX (CG-3M; model: 858011, serial No. 9507278) gravimeter at 1 km interval along the survey line. The number of measurement points was 151 (**Table 1**). Since the survey line was located over 100 km apart from the gravity reference point at Syowa Station (SYO; 69.0S, 39.6E), we set up two temporal gravity reference points at both S16 and H176. These reference points were linked to the absolute gravity point (IAGBN-A) at SYO and gravity values of the points were determined using the absolute gravity value of 982524.327 mgal [13]. In the gravity measurements, we did not adopt the closed loop method which was usually used in conventional gravity surveys. Instead, we carried out the gravity measurements more than twice at several stations including S16 and H176 reference points. If the three successive measurements agreed within a certain allowance revel (10 micro-gal), the final gravity value at the point was determined to be a mean value of these three measurements. The drift rate throughout the total measurement period of 48 days was 0.47 mgal/day and we found no significant jumps in reading the values. **Figure 2** shows the drift rate throughout the measurement period by joining the reading values at S16 and H176.

2.2. GPS Measurements

In order to determine precise positions of the gravity points, we used dual-frequency GPS (Ashtech Z type recievers). To determine coordinates of a point, we recorded 20 minutes GPS data for every 5 s sampling interval. The coordinates of almost the points were precisely calculated on the WGS-84 ellipsoid by rapid static positioning method between the each point and the permanent GPS station at SYO. In contrast, the coordinates of a few numbers of points were calculated by means of "autogipsy" on the basis of the global GPS database (http://gipsy.jpl.nasa.gov). **Figure 3** represents the errors in the positioning calculating procedure. Elevation errors in almost all points were achieved less than 0.3 m; which corresponds to the errors in free-air anomalies of about 0.1 mgal.
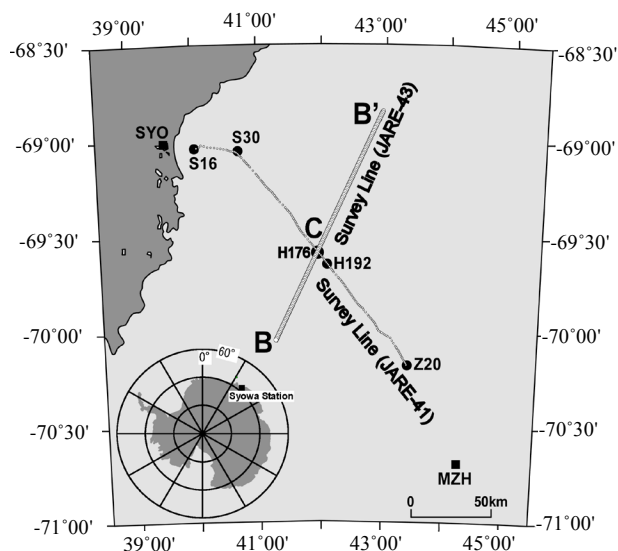

Figure 1. Map showing the JARE-43 gravity survey profile. Small open circles indicate 151 measurement points. Solid line denotes the JARE-41 survey profile. Large solid circles and squares show important route points (S16 and H176) and the Japanese Antarctic Stations (Syowa: SYO; Mizuho: MZH), respectively.
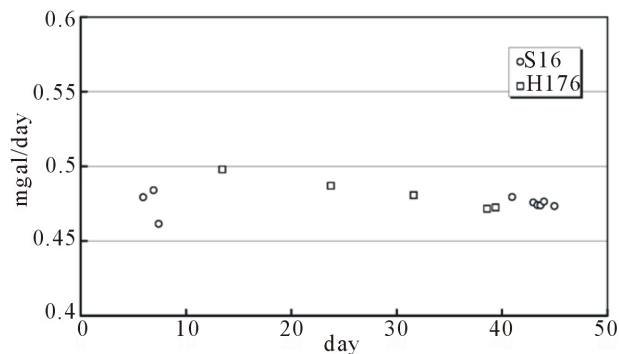

Figure 2. A drift rate throughout the measurement period in 2001-2002 survey. The approximately the same value in 0.47 mgal/day was obtained from both the results at S16 and H176 observation points.

S. TODA *ET AL.*

Table 1. Results of the gravity survey on the Mizuho Plateau in 2001-2002 operation by JARE-43.

Station	Latitude			Longitude			Altitude (m)	Gravity value (mgal)	Free Air anomaly (mgal)	Bedrock elevation Ice Rader (m)	Bouguer anomaly Ice Rader (mgal)	Bedrock elevation seismic (m)	Bouguer anomaly seismic (mgal)
	(deg)	(min)	(sec)	(deg)	(min)	(sec)							
HM001	70	3	51.3	41	14	34.7	1481.43	982172.66	16.9			0	−39.0
HM002	70	3	22.5	41	15	17.5	1480.92	982172.94	17.5			0	−38.4
HM003	70	2	53.5	41	16	0.5	1485.18	982171.44	17.7			0	−38.3
HM004	70	2	24.6	41	16	43.2	1488.04	982169.22	16.9			0	−39.3
HM005	70	1	55.8	41	17	26.3	1492.05	982166.66	16.0			−50	−36.4
HM006	70	1	26.9	41	18	9.1	1493.38	982164.54	14.8			−100	−33.8
HM007	70	0	58.1	41	18	51.4	1490.85	982163.78	13.7			−150	−30.9
HM008	70	0	29.2	41	19	34.5	1490.78	982164.38	14.8			−150	−29.9
HM009	70	0	0.2	41	20	16.9	1493.19	982165.16	16.7			−100	−31.8
HM010	69	59	31.4	41	21	0.2	1500.75	982165.38	19.8			−50	−33.0
HM011	69	59	2.6	41	21	42.6	1506.79	982166.97	23.7			0	−33.2
HM012	69	58	33.8	41	22	24.9	1506.15	982170.14	27.1			50	−33.6
HM013	69	58	5.0	41	23	8.8	1505.11	982172.22	29.3			100	−35.2
HM014	69	57	36.0	41	23	51.1	1502.94	982173.74	30.7			150	−37.7
HM015	69	57	7.2	41	24	33.8	1497.44	982175.06	30.8			150	−37.4
HM016	69	56	38.4	41	25	16.0	1488.23	982177.99	31.3			150	−36.5
HM017	69	56	9.5	41	25	58.8	1489.43	982179.38	33.6			150	−34.3
HM018	69	55	40.5	41	26	40.5	1490.83	982180.59	35.7			150	−32.2
HM019	69	55	11.4	41	27	23.1	1498.42	982177.04	34.9			150	−33.2
HM020	69	54	42.6	41	28	5.3	1512.29	982170.20	32.8			150	−35.9
HM021	69	54	13.6	41	28	48.1	1515.35	982165.74	29.8			150	−39.0
HM022	69	53	44.7	41	29	30.2	1516.96	982162.41	27.4			100	−37.6
HM023	69	53	15.9	41	30	12.7	1518.47	982158.74	24.7			50	−36.5
HM024	69	52	46.9	41	30	55.2	1516.81	982155.72	21.6			0	−35.6
HM025	69	52	18.0	41	31	37.3	1513.97	982154.90	20.4			0	−36.7
HM026	69	51	48.9	41	32	19.4	1511.86	982155.02	20.4			0	−36.7
HM027	69	51	20.1	41	33	1.7	1509.17	982155.05	20.0			0	−36.9
HM028	69	50	51.2	41	33	43.8	1509.89	982154.11	19.8			0	−37.2
HM029	69	50	22.3	41	34	26.1	1509.54	982153.60	19.6			0	−37.3
HM030	69	49	53.2	41	35	8.0	1511.58	982152.65	19.8			0	−37.2
HM031	69	49	24.3	41	35	50.3	1514.72	982150.38	19.0			0	−38.2
HM032	69	48	55.4	41	36	31.6	1516.80	982148.50	18.2			0	−39.0
HM033	69	48	26.5	41	37	14.0	1517.97	982147.13	17.6			0	−39.6
HM034	69	47	57.4	41	37	55.8	1516.14	982146.77	17.2			0	−40.0
HM035	69	47	28.5	41	38	38.0	1514.45	982146.87	17.3			0	−39.9
HM036	69	46	59.7	41	39	19.5	1516.51	982146.44	17.9			0	−39.3
HM037	69	46	30.5	41	40	1.3	1519.57	982145.95	18.9			0	−38.5
HM038	69	46	1.8	41	40	43.5	1517.78	982145.67	18.5			0	−38.8

Continued

HM039	69	45	32.7	41	41	24.9	1518.99	982145.64	19.3			0	−38.0
HM040	69	45	3.6	41	42	6.9	1517.05	982146.68	20.2			−10	−36.2
HM041	69	44	34.6	41	42	48.3	1516.95	982147.48	21.5			−20	−34.4
HM042	69	44	5.6	41	43	30.1	1522.00	982146.05	22.1	111	−43.0	−30	−33.3
HM043	69	43	36.6	41	44	11.7	1525.17	982143.41	20.9	43	−39.6	−40	−33.9
HM044	69	43	7.7	41	44	53.8	1529.98	982141.25	20.7	77	−42.3	−50	−33.6
HM045	69	42	38.6	41	45	35.4	1531.50	982140.01	20.4	24	−39.0	−60	−33.2
HM046	69	42	9.8	41	46	17.3	1534.12	982138.87	20.5	28	−39.3	−70	−32.5
HM047	69	41	40.7	41	46	58.3	1537.46	982137.92	21.1	67	−41.6	−80	−31.4
HM048	69	41	11.6	41	47	40.0	1541.28	982137.25	22.1	47	−39.3	−90	−29.8
HM049	69	40	42.7	41	48	21.8	1545.37	982136.27	22.8	94	−41.9	−100	−28.5
HM050	69	40	13.6	41	49	2.7	1547.32	982135.03	22.7	160	−46.8	−100	−28.8
HM051	69	39	44.6	41	49	44.0	1547.96	982133.44	21.8	84	−42.5	−90	−30.4
HM052	69	39	15.6	41	50	25.9	1549.11	982131.33	20.5	57	−41.9	−80	−32.4
HM053	69	38	46.5	41	51	7.0	1547.01	982129.56	18.5	7	−40.3	−70	−35.0
HM054	69	38	17.6	41	51	48.6	1545.26	982127.91	16.8	39	−44.2	−60	−37.3
HM055	69	37	48.6	41	52	29.4	1544.69	982126.51	15.7	12	−43.4	−50	−39.1
HM056	69	37	19.5	41	53	10.8	1547.78	982124.90	15.6	32	−45.0	−50	−39.4
HM057	69	36	50.4	41	53	52.3	1547.49	982123.67	14.7	13	−44.6	−50	−40.2
HM059	69	36	21.4	41	54	33.3	1547.06	982122.59	14.0	19	−45.7	−50	−40.9
HM061	69	35	52.4	41	55	14.4	1547.99	982120.61	12.8	57	−49.6	−50	−42.2
HM063	69	35	23.5	41	55	55.9	1550.24	982117.27	10.6	−30	−45.8	−50	−44.4
HM065	69	34	54.3	41	56	37.6	1550.96	982113.49	7.5	−60	−46.9	−150	−40.6
HM067	69	34	24.9	41	57	16.0	1553.44	982109.67	4.9	−94	−47.1	−250	−36.4
HM069	69	33	56.5	41	57	59.0	1553.80	982106.31	2.2	−176	−44.3	−350	−32.2
HM071	69	33	27.5	41	58	40.2	1550.59	982104.30	−0.3	−266	−40.4	−450	−27.7
HM073	69	32	58.5	41	59	21.4	1544.32	982103.26	−2.9	−500	−26.5	−550	−23.1
HM075	69	32	29.4	42	0	2.0	1539.90	982103.34	−3.7	−300	−41.0	−550	−23.7
HM077	69	32	0.4	42	0	43.0	1538.63	982105.54	−1.4	−200	−45.6	−450	−28.3
HM078	69	31	31.3	42	1	24.0	1540.19	982109.46	3.5	−88	−48.5	−350	−30.4
HM079	69	31	2.2	42	2	4.8	1541.09	982113.12	7.9	−31	−48.1	−250	−32.9
HM080	69	30	33.2	42	2	45.6	1542.40	982115.24	10.9	10	−47.9	−150	−36.9
HM081	69	30	4.1	42	3	26.7	1543.00	982115.99	12.4	17	−47.0	−100	−38.9
HM082	69	29	35.0	42	4	7.4	1543.18	982116.17	13.1	−30	−43.1	−100	−38.2
HM083	69	29	5.9	42	4	48.0	1543.04	982116.36	13.7	−46	−41.4	−100	−37.6
HM084	69	28	36.9	42	5	28.8	1543.01	982116.60	14.4	−49	−40.4	−100	−36.9
HM085	69	28	7.9	42	6	9.7	1541.04	982117.18	14.9	−4	−43.0	−100	−36.4
HM086	69	27	38.7	42	6	50.5	1541.52	982117.11	15.4	−1	−42.6	−100	−35.8
HM087	69	27	9.6	42	7	30.7	1539.34	982116.89	15.0	8	−43.6	−100	−36.1
HM088	69	26	40.7	42	8	11.6	1538.05	982116.47	14.7	−49	−40.0	−50	−39.9
HM089	69	26	11.5	42	8	52.1	1535.83	982116.06	14.1	−46	−40.7	0	−43.9

Continued

HM090	69	25	42.5	42	9	32.5	1534.79	982116.21	14.4	4	−43.8	10	−44.2
HM091	69	25	13.3	42	10	12.8	1534.00	982116.97	15.4	−9	−41.9	20	−43.9
HM092	69	24	44.4	42	10	53.3	1535.50	982117.93	17.3	13	−41.5	30	−42.7
HM093	69	24	15.3	42	11	33.6	1539.70	982118.50	19.6	96	−45.1	40	−41.2
HM094	69	23	46.2	42	12	14.0	1543.21	982119.39	22.1	223	−51.6	50	−39.6
HM095	69	23	17.0	42	12	54.2	1542.25	982120.52	23.4	222	−50.2	40	−37.5
HM096	69	22	48.0	42	13	34.7	1542.55	982119.49	23.0	99	−42.1	30	−37.3
HM097	69	22	18.9	42	14	14.9	1547.09	982117.15	22.5	−8	−35.3	20	−37.3
HM098	69	21	49.8	42	14	55.3	1548.96	982116.15	22.6	65	−40.4	10	−36.6
HM099	69	21	20.8	42	15	35.8	1545.24	982115.21	21.0	−2	−37.2	0	−37.3
HM100	69	20	51.7	42	16	15.7	1545.05	982113.31	19.5	−54	−35.1	−10	−38.1
HM101	69	20	22.2	42	16	56.0	1544.12	982111.76	18.1	−92	−33.8	−20	−38.7
HM102	69	19	53.1	42	17	35.8	1544.66	982111.40	18.4	−88	−33.8	−30	−37.8
HM103	69	19	24.1	42	18	15.3	1542.02	982112.34	19.0	−25	−37.4	−40	−36.4
HM104	69	18	54.8	42	18	56.9	1542.57	982113.10	20.5	11	−38.5	−50	−34.3
HM105	69	18	25.8	42	19	36.5	1541.85	982112.77	20.4	21	−39.2	−60	−33.6
HM106	69	17	56.7	42	20	16.4	1540.93	982111.73	19.6	0	−38.6	−70	−33.7
HM107	69	17	27.5	42	20	56.5	1537.29	982111.12	18.3	6	−40.1	−80	−34.2
HM108	69	16	58.4	42	21	36.5	1531.40	982110.78	16.6	17	−42.3	−90	−34.9
HM109	69	16	29.3	42	22	16.3	1527.85	982109.24	14.5	−57	−39.2	−90	−36.9
HM110	69	16	0.1	42	22	56.1	1527.84	982107.22	12.9	−64	−40.3	−80	−39.2
HM111	69	15	31.0	42	23	35.9	1526.91	982105.483	11.4	−46	−43.0	−70	−41.4
HM112	69	15	1.9	42	24	16.0	1526.72	982104.262	10.6	−43	−44.0	−60	−42.8
HM113	69	14	32.8	42	24	55.6	1524.70	982103.030	9.2	−99	−41.4	−50	−44.8
HM114	69	14	3.8	42	25	35.2	1522.35	982102.393	8.4	−97	−42.4	−40	−46.3
HM115	69	13	34.6	42	26	15.0	1521.31	982102.201	8.3	−99	−42.2	−30	−47.0
HM116	69	13	5.5	42	26	54.8	1521.06	982103.155	9.7	−54	−43.9	−20	−46.3
HM117	69	12	36.1	42	27	34.5	1519.11	982106.105	12.6	159	−55.7	−10	−44.1
HM118	69	12	7.0	42	28	14.1	1511.40	982110.061	14.6	180	−54.8	0	−42.4
HM119	69	11	37.9	42	28	54.1	1507.74	982112.288	16.2	149	−51.0	10	−41.4
HM120	69	11	8.6	42	29	33.4	1505.56	982113.422	17.2	260	−57.6	20	−41.0
HM121	69	10	39.5	42	30	13.2	1500.14	982113.896	16.4	162	−51.3	30	−42.2
HM122	69	10	10.5	42	30	52.6	1498.78	982112.755	15.4	94	−47.7	40	−43.9
HM123	69	9	41.4	42	31	32.4	1498.80	982111.607	14.7	96	−48.5	50	−45.3
HM124	69	9	12.2	42	32	12.0	1498.56	982110.848	14.4	76	−47.4	60	−46.3
HM125	69	8	43.1	42	32	51.3	1495.38	982110.460	13.5	61	−47.1	70	−47.8
HM126	69	8	13.8	42	33	30.6	1494.97	982109.927	13.3	74	−48.2	80	−48.6
HM127	69	7	44.6	42	34	10.0	1492.44	982110.689	13.8	134	−51.8	90	−48.7
HM128	69	7	15.4	42	34	49.3	1483.77	982112.676	13.6	211	−57.0	100	−49.3
HM129	69	6	46.3	42	35	28.7	1477.42	982111.564	11.0	54	−48.5	0	−44.7
HM130	69	6	17.2	42	36	8.2	1481.02	982108.487	9.5	21	−47.8	−100	−39.4

Continued

HM131	69	5	48.0	42	36	47.3	1474.92	982108.761	8.4	76	−52.5	−150	−36.8
HM132	69	5	18.9	42	37	26.8	1468.02	982108.224	6.3	13	−50.0	−200	−35.3
HM133	69	4	49.6	42	38	6.0	1464.64	982107.506	5.0	11	−51.0	−200	−36.4
HM134	69	4	20.3	42	38	45.0	1461.16	982107.179	4.1	−16	−49.9	−200	−37.2
HM135	69	3	51.0	42	39	24.2	1459.68	982106.803	3.7	−46	−48.1	−200	−37.5
HM136	69	3	21.7	42	40	3.4	1458.36	982107.003	4.0	−24	−49.3	−200	−37.2
HM137	69	2	52.7	42	40	42.4	1454.28	982108.234	4.5	−9	−49.7	−200	−36.5
HM138	69	2	23.5	42	41	21.6	1448.60	982109.120	4.1	−25	−48.8	−200	−36.7
HM139	69	1	54.2	42	42	0.5	1445.78	982109.512	4.1	−62	−46.1	−250	−33.1
HM140	69	1	25.1	42	42	39.8	1444.90	982109.872	4.7	−86	−43.8	−300	−29.0
HM141	69	0	56.0	42	43	18.8	1438.80	982111.213	4.7	−77	−44.3	−300	−28.9
HM142	69	0	26.6	42	43	57.8	1433.41	982112.780	5.1	−82	−43.3	−300	−28.3
HM143	68	59	57.4	42	44	36.6	1426.48	982114.610	5.3	−83	−42.8	−300	−27.8
HM144	68	59	28.3	42	45	15.3	1418.87	982117.180	6.0	−66	−43.0	−300	−26.8
HM145	68	58	59.1	42	45	54.5	1413.31	982118.629	6.2	−105	−39.9	−300	−26.4
HM146	68	58	29.8	42	46	33.4	1405.54	982121.219	6.9	−131	−37.1	−300	−25.4
HM147	68	58	0.6	42	47	12.3	1395.89	982124.815	8.0	−127	−35.9	−300	−23.9
HM148	68	57	31.4	42	47	51.1	1380.02	982129.407	8.2	−148	−33.7	−300	−23.1
HM149	68	57	2.2	42	48	30.3	1380.86	982130.081	9.6	−179	−30.1	−300	−21.7
HM150	68	56	33.0	42	49	8.8	1385.28	982130.351	11.7	−121	−32.2	−300	−19.8
HM151	68	56	3.7	42	49	47.2	1385.62	982132.587	14.6	−56	−33.8	−300	−16.9
HM152	68	55	34.5	42	50	26.0	1376.05	982137.670	17.2	0	−34.7	−300	−14.0
HM153	68	55	5.3	42	51	4.6	1363.90	982141.900	18.2	−44	−30.2	−250	−16.0
HM154	68	54	36.0	42	51	43.4	1362.05	982143.239	19.5	−41	−29.1	−200	−18.1
HM155	68	54	6.7	42	52	21.7	1363.06	982144.052	21.1	−28	−28.4	−150	−20.0
HM156	68	53	37.4	42	53	0.2	1358.70	982145.216	21.4	24	−31.5	−100	−23.0
HM157	68	53	8.3	42	53	38.8	1351.77	982146.316	20.9	18	−31.4	−50	−26.7
HM158	68	52	39.1	42	54	17.4	1346.07	982145.976	19.2	−47	−28.3	0	−31.5
HM159	68	52	9.7	42	54	56.0	1345.29	982144.863	18.4	−91	−26.1	50	−35.8
HM160	68	51	40.6	42	55	34.2	1344.27	982144.619	18.3	−60	−28.2	100	−39.3
HM161	68	51	11.3	42	56	13.0	1339.19	982145.510	18.1	−58	−28.3	100	−39.3

3. Gravity Anomaly Calculations

3.1. Methods

The Free-air anomaly Δg is calculated by the following formula,

$$\Delta g = g - \gamma + 0.30839H + 0.87 - 0.0000965H$$

where g is the measured gravity value (in mgal), γ is the normal gravity defined on the reference ellipsoid 1980 (in mgal), and H is the WGS-84 ellipsoidal height of the gravity point (in meter). Then, the simple Bouguer anomaly $\Delta g'$ is calculated by the formula,

$$\Delta g' = \Delta g - z\pi G \left\{ \rho_i (H - h) + \rho_c h \right\},$$

where G is the Newton's gravitational constant, ρ_c is the density of bedrock assumed to be 2.55 or 2.75 g/cm^3 so as to correspond to the final density models; ρ_i is the density of the ice assuming as 0.9 g/cm^3, and h is the elevation of the bedrock in meter.

3.2. Ice-Sheet Surface and Bedrock Elevations

In order to calculate the simple Bouguer anomaly, it is necessary to remove the effect of the ice-sheet overlaying
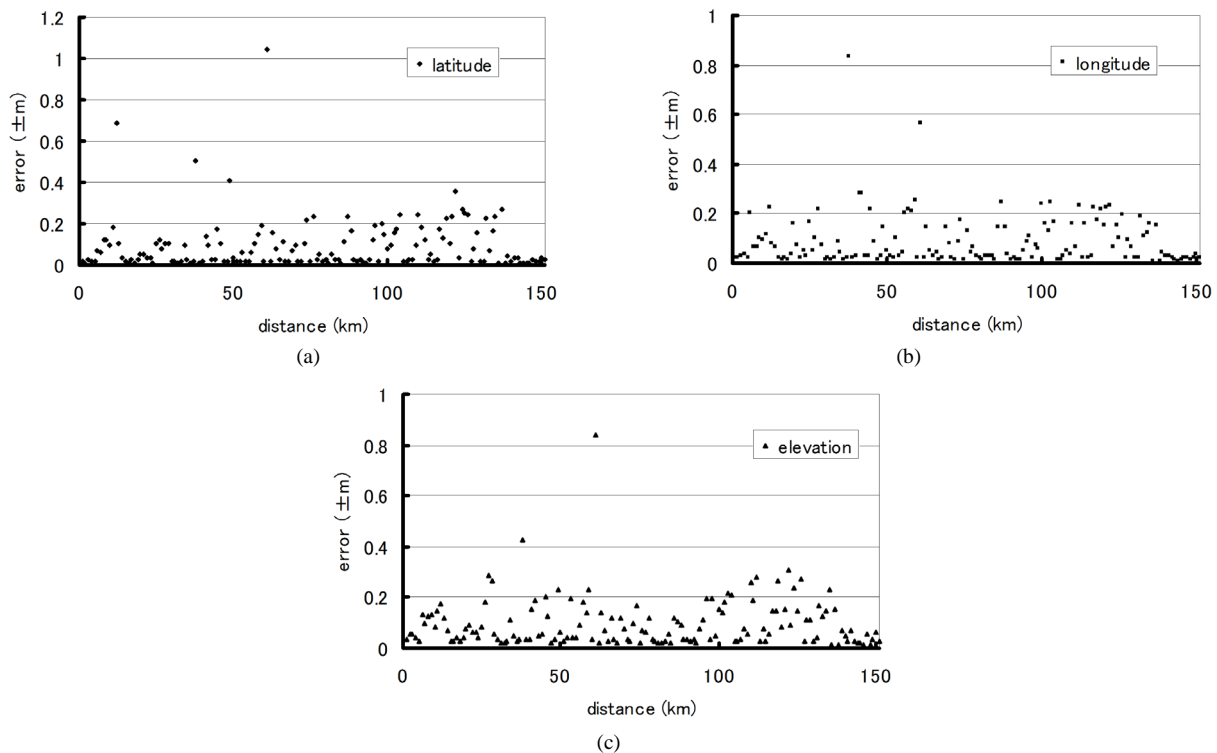
Figure 3. Calculated GPS positioning errors of all stations. ((a) latitude; (b) longitude; (c) elevation).

the bedrock surface. Two kinds of dataset for the bedrock elevation (that is reduced from ice-sheet surface to the ice-sheet thickness) beneath the survey line are available. The one is a result from the radio-echo sounding simultaneously conducted at the survey ([14], **Figure 4**), the other is obtained from seismic travel-time analysis [15]. **Figure 5** shows the distribution of surface elevation and bedrock elevation of these two data sets. It is clear that the bedrock elevations obtained by seismic travel-time analysis is generally deeper than those obtained by the radio-echo sounding. It is noted that the maximum errors technically anticipated are 100 m for the radio-echo sounding [16], and 350 m for the seismic data [10]: These maximum elevation errors could firmly produce the Bouguer anomalies about 7 mgal and 25 mgal, respectively.

It is also noted that the bedrock elevations from radio-echo sounding were not actually determined at several points, due to a mechanical trouble of the radar instrument. Moreover, there were several places where no reflected signals from the bedrock by the radio-echo sounding, in particular around the points over the furrowed bedrock topography in central part of the profile (point C in **Figure 5**, the cross-section between two profiles by JARE-41 and -43). This furrowed bedrock topography was also observed at the Mizuho traverse routes by both the radio-echo sounding and the seismic travel-times for JARE-41 analyses [10,16]. Unfortunately, it may be difficult to make accurate evaluation for which

elevation model could be geophysically and glaciologically more plausible. Therefore, in this paper, we shall calculate the simple Bouguer gravity anomalies by applying for both these two bedrock elevation models.

3.3 Free-Air and Bouguer Anomalies

Table 1 shows the coordinates, observed gravity values, obtained Free-air and Bouguer anomalies, together with bedrock elevations at the gravity measured points. Free-air and Bouguer gravity anomalies are also illustrated in **Figures 5** and **6**, respectively. **Figure 5** indicates a fine correlation between the Free-air gravity anomalies and the bedrock topography along the profile. Free-air gravity anomaly varies in +38 and −3 mgal. Furrowed negative free-air anomalies around H176 (point C in **Figure 5**) implies an existence of a valley structure as seen in the same manner for the bedrock topography. Around this valley, there is no reflected signal recorded from the bedrock by the radio-echo sounding data.

The calculated Bouguer gravity anomalies varies in −10 to −60 mgal (**Figure 6**). Variation in Bouguer anomalies in adjacent measurement points might be caused chiefly by those of bedrock elevation retrieved from both radio-echo soundings and seismic surveys. Hereafter, therefore, we discuss about the characteristics of Bouger anomalies in long period wave-length over few tens of km while constructing the crustal density models. The short-period wavelength variations in Bouguer anomalies
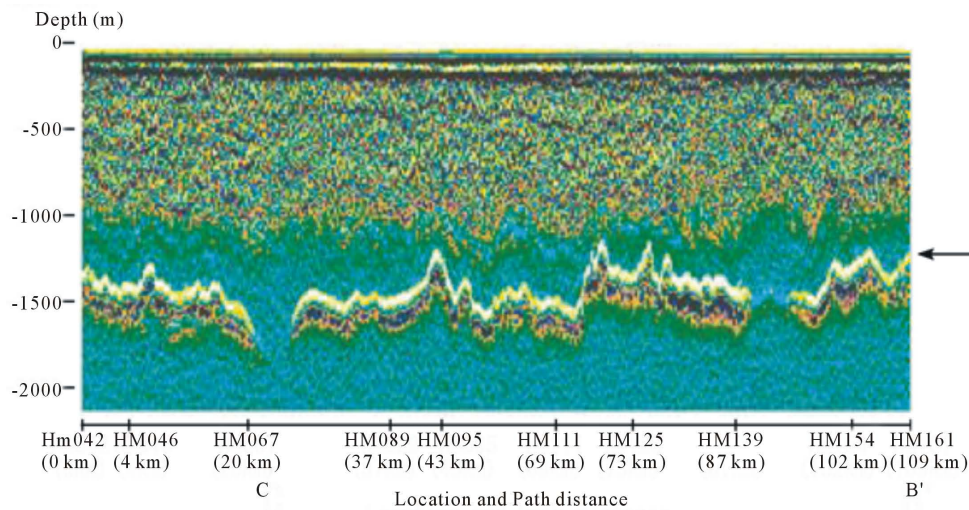
Figure 4. Reflection images of inner structure for the ice-sheet and bedrock topography obtained from radio-echo sounding along the seismic/gravity profile [14]. Black arrow (right hand side in the figure) indicates the reflected echoes from the bedrock surface.
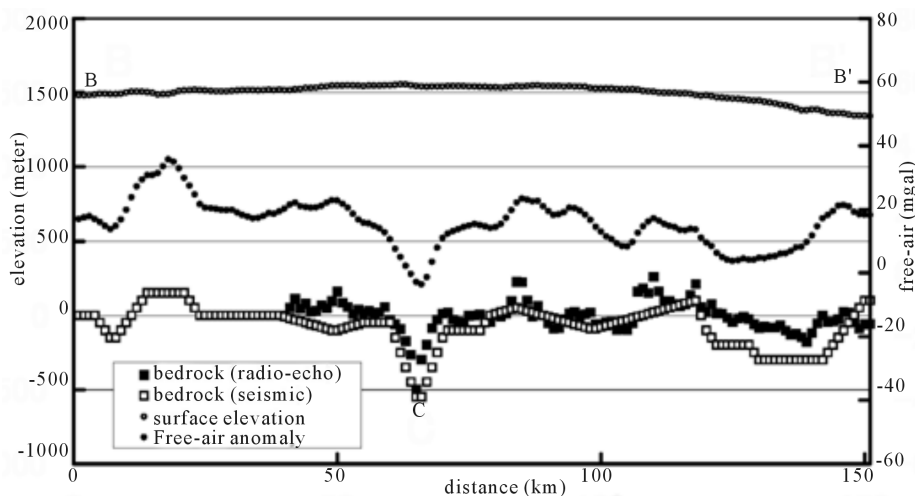

Figure 5. Surface elevation and bedrock topography, together with Free-air gravity anomalies along the survey profile. Small open circles indicate surface elevation determined by GPS measurements. Large solid and open squares indicate the bedrock topography obtained from radio-echo sounding [14] and from the seismic refraction survey [15], respectively. Small solid circles indicate the Free-air gravity anomalies.
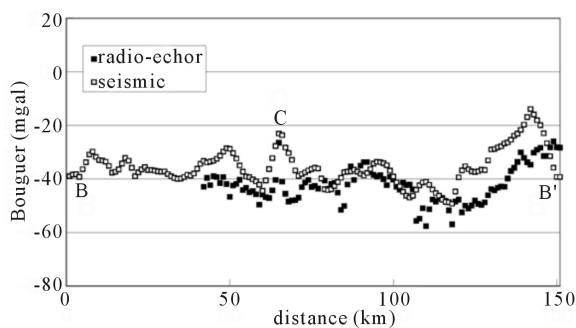
Figure 6. Bouguer gravity anomalies along the survey profile. Solid and open squares indicate the anomalies calculated from the radio-echo sounding [14] and from the seismic refraction survey [15], respectively.

supposed to be caused by the small scale heterogeneity in topmost crustal layer including sediments, otherwise a mixture layer composed from ice and moraine rocks spreading over the bedrock beneath continental ice sheet. The negative gravity anomaly suggests the evidence of the thick crust, or the existence of low-density materials are underlying. The Bouguer anomalies in the south and the central parts of the profile have not so much variations and it means that the density discontinuity of the deeper part of the crust could be in less horizontal variation. On the contrary, the low velocity zone in the upper crust at the northern profile (B' in **Figure 6**) is implied by the increasing Bouguer anomalies. A "ridge shaped" Bouguer anomalies at H176 (C in **Figure 6**) is probably

related to the underlying furrowed bedrock topography.

4. Discussion

As a main program of the SEAL deep exploration in austral summer in 2001-2002 by JARE-43, wide-angle reflection and refraction survey was carried out along the seismic profile on the Mizuho Plateau. [15] proposed velocity variations and three prominent seismic velocity boundaries along the profile. The P-wave velocities of the upper crust was identified to have lateral variations of 5.9 km/s in the north, 6.0 km/s around the point C (H176), and 6.1 - 6.2 km/s in the center and south of the profile. The first boundary was determined by reflection phases at 19 km in depth between the upper and the middle crust. The second boundary was recognized by reflected waves from the lower crust at 30 km in depths. The third boundary was determined by prominent reflection phases from the Moho at 40 km in depths. However, the inclination of the Moho boundaries are not identified without any significant seismic phase information, because they cannot detect the refracted waves from the Moho (Pn waves) by the experiment caused by the short length less than 200 km over the whole profile. Shallow part of the crust velocity model by [15] corresponds to the gravity-based model from this study. Lateral variations in P-wave velocities in the upper crust can be explained by assuming the low-density material in the topmost crust. For further study, we might investigate the validity of this boundary's variation by means of a comparison with the other available geophysical data such as geomagnetic anomalies, satellite gravity, together with detail reflection imaging.

5. Conclusion

A gravity survey was carried out on the Mizuho Plateau as one of the geophysical measurements by the SEAL exploration in 2001-2002. The gravity measurements were conducted along the seismic profile of 150 km in length. Free-air and Bouguer anomalies were calculated using the precise locations determined by GPS observations, by considering the effect of thick ice-sheet. The furrowed and basin-like negative Free-air anomalies were obtained in the central and northern parts of the profile. The crustal thickness was demonstrated so as to fit the observed Bouguer anomalies. Our gravimetric results are almost corresponding to the P-wave velocity structure by refraction and wide-angle reflection study [15].

Acknowledgements

REFERENCES

[1] Y. Hiroi, K. Shiraishi and Y. Motoyoshi, "Late Proterozoic Paired Metamorphic Complexes in East Antarctica, with Special Reference to the Tectonic Significance of Ultramafic Rocks," In: M. R. A. Thomson, *et al.*, Eds., *Geological Evolution of Antarctica*, Cambridge University Press, Cambridge, 1991, pp. 83-87.

[2] K. Yanai and S. Kaminuma, "Measurement of Gravity along the Traverse Routes Syowa-South Pole," *JARE Sci. Rep.*, *Spec.*, Vol. 2, 1971, pp. 131-150.

[3] T. Nagao and K. Kaminuma, "Gravity Survey in the Mizuho Plateau," *JARE Data Reports*, Vol. 132, 1988, pp. 1-32.

[4] K. Kamiyama, T. Furukawa, H. Maeno, T. Kishi and M. Kanao, "Glaciological Data Collected by the 33rd Japanese Antarctic Research Expedition in 1992," *JARE Data Reports*, Vol. 194, 1994, pp. 1-67.

[5] T. Higashi, M. Kanao, H. Motoyama and T. Yamanouchi, "Gravity Observations along the Traverse Routes from Syowa Station to Dome Fuji Station, East Antarctica," *Polar Geoscience*, Vol. 14, 2001, pp. 226-234.

[6] M. Kanao, K. Kamiyama and K. Ito, "Crustal Density Structure of the Mizuho Plateau, East Antarctica from Gravity Survey in 1992," *Polar Geoscience*, Vol. 7, 1994, pp. 23-36.

[7] M. Kanao, M. Ishikawa, M. Yamashita, K. Kaminuma and L. D. Brown, "Structure and Evolution of the East Antarctic Lithosphere: Tectonic Implications for the Development and Dispersal of Gondwana," *Gondwana Research*, Vol. 7, No. 1, 2004, pp. 31-41.
http://dx.doi.org/10.1016/S1342-937X(05)70304-X

[8] M. Kanao, A. Fujiwara, H. Miyamachi, S. Toda, M. Tomura, K. Ito and T. Ikawa, "Reflection Imaging of the Crust and the Lithospheric Mantle in the Lützow-Holm Complex, Eastern Dronning Maud Land, Antarctica, Derived from the SEAL Transects," *Tectonophysics*, Vol. 508, No. 1-4, 2011, pp. 73-84.
http://dx.doi.org/10.1016/j.tecto.2010.08.005

[9] H. Miyamachi, H. Murakami, T. Tsutsui, S. Toda, T. Minta and M. Yanagisawa, "A Seismic Refraction Experiment in 2000 on the Mizuho Plateau, East Antarctica (JARE-41)," *Antarctic Report*, Vol. 45, 2001, pp. 101-147.

[10] T. Tsutsui, H. Murakami, H. Miyamachi, S. Toda and M. Kanao, "P-Wave Velocity Structure of the Ice Sheet and the Shallow Crust Beneath the Mizuho Traverse Routes, East Antarctica, from Seismic Refraction Analysis," *Polar Geoscience*, Vol. 14, 2001, pp. 195-211.

[11] S. Toda, H. Miyamachi, H. Murakami, T. Tsutsui and M. Kanao, "Gravity Survey along the Mizuho Traverse Routes, East Antarctica: SEAL Seismic Exploration in 1999-2000," *International Journal of Geosciences*, Vol. 4, No. 10, 2013, pp. 1392-1400.
http://dx.doi.org/10.4236/ijg.2013.410136

[12] H. Miyamachi, S. Toda, T. Matsushima, M. Takada, Y. Takahashi, D. Kamiya, A. Watanabe, M. Yamashita and M. Yanagisawa, "A Seismic Refraction and Wide-Angle Reflection Exploration in 2002 on the Mizuho Plateau, East Antarctica," *Antarctic Report*, Vol. 47, 2003, pp. 32-71.

[13] K. Kaminuma, K. Tsukahara and S. Takemoto, "Absolute Gravity Value Measured at Syowa Station, Antarctica," *Bulletin of the D'Information BGI*, Vol. 80, 1997, pp. 26-29.

[14] M. Takada, S. Toda, D. Kamiya and H. Miyamachi, "The Ice Radar Survey along the JARE-43 Seismic Exploration Profile in the Mizuho Plateau, East Antarctica," *Antarctic Report*, Vol. 47, 2003, pp. 380-394.

[15] H. Miyamachi, S. Toda, T. Matsushima, M. Takada, A. Watanabe, M. Yamashita and M. Kanao, "Seismic Refraction and Wide-Angle Reflection Exploration by JARE-43 on Mizuho Plateau, East Antarctica," *Polar Geoscience*, Vol. 16, 2003, pp. 1-21.

[16] H. Maeno, K. Kamiyama, T. Furukawa, O. Watanabe, R. Naruse, K. Okamoto, T. Suitz and S. Uratsuka, "Using a Mobile Radio Echo Sounder to Measure Bedrock Topography in East Queen Maud Land, Antarctica," *Polar Meteorology and Glaciology*, Vol. 8, 1994, pp. 149-160.